Proline Scan of the hERG Channel S6 Helix Reveals the Location of the Intracellular Pore Gate

Samrat Thouta, Stanislav Sokolov, Yuki Abe, Sheldon J. Clark, Yen M. Cheng, and Tom W. Claydon*
Department of Biomedical Physiology and Kinesiology, Simon Fraser University, Burnaby, BC, Canada

ABSTRACT In *Shaker*-like channels, the activation gate is formed at the bundle crossing by the convergence of the inner S6 helices near a conserved proline-valine-proline motif, which introduces a kink that allows for electromechanical coupling with voltage sensor motions via the S4-S5 linker. Human ether-a-go-go-related gene (hERG) channels lack the proline-valine-proline motif and the location of the intracellular pore gate and how it is coupled to S4 movement is less clear. Here, we show that proline substitutions within the S6 of hERG perturbed pore gate closure, trapping channels in the open state. Performing a proline scan of the inner S6 helix, from Ile^{655} to Tyr^{667} revealed that gate perturbation occurred with proximal (I655P-Q664P), but not distal (R665P-Y667P) substitutions, suggesting that Gln^{664} marks the position of the intracellular gate in hERG channels. Using voltage-clamp fluorimetry and gating current analysis, we demonstrate that proline substitutions trap the activation gate open by disrupting the coupling between the voltage-sensing unit and the pore of the channel. We characterize voltage sensor movement in one such trapped-open mutant channel and demonstrate the kinetics of what we interpret to be intrinsic hERG voltage sensor movement.

INTRODUCTION

The human *KCNH2* gene encodes the pore-forming α-subunit of the cardiac voltage-gated K^+ (Kv) channel Kv11.1 or human-ether-a-go-go-related gene (hERG). hERG channels underlie the rapid delayed rectifier current, I_{Kr}, in the heart that is essential for repolarization of the cardiac action potential and consequently normal cardiac electrical activity and rhythm (1,2). In contrast to other Kv channels, hERG channels display unusual gating characteristics, which include slow activation and rapid voltage-dependent inactivation that restrict repolarizing current upon initial membrane depolarization, and slow deactivation and rapid recovery from inactivation that allow channels to revisit and dwell in the open state upon repolarization, thus producing a resurgent repolarizing current that aids terminal repolarization of the action potential. Despite orchestrating such a unique role for hERG channels in cardiac physiology, the mechanisms underlying the unusual gating behaviors in hERG channels are not well understood. In particular, neither the location of the intracellular pore gate, nor the manner in which it is coupled to the voltage-sensing unit of the channel, are well defined. This is of principal interest, because hERG channels are targeted by many pharmaceutical agents, the majority of which block by entering the pore via the intracellular activation gate and are limited by the unusually slow opening of the pore gate. Drug binding that reduces hERG channel function, as with congenital mutations, has been shown to prolong the duration of the action potential and lead to long QT syndrome, a potentially life-threatening ventricular repolarization disorder that is associated with increased vulnerability to arrhythmia, ventricular fibrillation, and sudden cardiac death (3,4). Moreover, recent advances in the discovery of hERG channel openers as therapeutics have identified sites of action that involve direct interactions with the voltage-sensing unit that may modify activation/deactivation gating (5). These observations underscore the need to understand the structural determinants of the hERG channel pore gate and the mechanistic basis of electromechanical coupling in these channels.

Evidence for gated access to the K^+ channel pore comes from reports of state-dependent blockade by intracellular quaternary ammonium derivatives, which blocked the open channel pore and could even be trapped by closure of the activation gate (6–9). In *Shaker* channels, the location of the activation gate was defined by examining state-dependent accessibility of engineered cysteines within S6 to methanethiosulfonate reagents and Cd^{2+} (10,11). These results showed that modification of Val^{478} occurred in both closed and open states, but that access was limited to the open state for sites deeper within the pore. Mutagenesis of S6 residues to small, bulky, or charged side chains helped to confirm Val^{478} and/or Phe^{481} as candidates for the *Shaker* gate (12). These data were corroborated by evidence that the gate could be trapped in the closed conformation by introducing tryptophan at Val^{478}, which suggested that Val^{478} forms a hydrophobic seal at the lower limit of the pore gate that acts as a steric barrier for K^+ permeation (13). Such functional evidence for the location of the gate is consistent with evidence from structures crystallized in open and closed states (14–16), which suggest that ion conduction is gated by the opening of an intracellular pore gate created as the lower S6 helices swing away from the midline of the pore (15). In Kv

Submitted August 29, 2013, and accepted for publication January 23, 2014.
*Correspondence: thomas_claydon@sfu.ca
Editor: William Kobertz.

0006-3495/14/03/1057/13 $2.00
http://dx.doi.org/10.1016/j.bpj.2014.01.035

channels, a conserved Pro-Val-Pro (PVP) motif introduces a kink in the S6 helices that brings them into contact with the S4-S5 linker to provide electromechanical coupling between voltage sensor movements and the S6 pore gate (16,17). Disruption of the highly conserved PVP motif dramatically alters gating, suggesting that it contributes to the structural form of the intracellular gate (12), one helical turn above the Val^{478} steric barrier.

hERG channels lack the S6 PVP motif raising questions as to the location of the gate and how it is coupled to voltage sensor movement. One study using a cysteine scan approach showed that inner hERG S6 helix mutations could alter gate function, primarily by disrupting the energetics of channel closing, resulting in a standing conductance at negative voltages (18). Interestingly, mutation of Ser^{660} (which corresponds to *Shaker* Val^{478}) did not alter hERG gating suggesting that the location of the activation gate may be different in hERG channels. This is consistent with a brief report that introduction of PVP into hERG channels prevented channel closure (19). Here, we define the location of the hERG activation gate by introducing a proline-induced kink at positions along the length of the inner S6 helix from, Ile^{655} to Tyr^{667}. Examining the pattern of gate perturbation by the engineered proline enabled us to define the boundary of the activation gate as, Gln^{664}, more than one full helical turn below the gate position in *Shaker*-like Kv channels. Voltage-clamp fluorimetry (VCF) and gating current data show that proline introduction disrupts coupling of voltage sensor movement with the pore gate, isolating the gate and trapping it in the open state. We characterize these reports of voltage sensor movement and charge transfer in a trapped-open channel, and show that a component of voltage sensor movement appears to be intrinsically slow in hERG channels expressed in *Xenopus* oocytes.

MATERIALS AND METHODS

Molecular biology

hERG channel constructs were incorporated into the pBluescript SKII vector and expressed in *Xenopus laevis* oocytes. Mutations were engineered using conventional overlap extension polymerase chain reaction with primers synthesized by Sigma Genosys (Oakville, Ontario). All mutant constructs were sequenced using Eurofins MWG Operon (Huntsville, AL) to ensure no errors were integrated during polymerase chain reaction cycles. Wild-type (WT) and mutant constructs were linearized using *XbaI* restriction endonuclease and cRNA was transcribed in vitro using the mMessage mMachine T7 Ultra cRNA transcription kit (Ambion, Austin, TX).

Oocyte preparation and injection

In accordance with Simon Fraser University Animal Care Committee and Canadian Council on Animal Care protocols and procedures, oocytes were isolated from female *X. laevis* frogs that were terminally anesthetized by immersion in 2 g/L tricaine solution (Sigma Aldrich) for 10–15 min. Selection and injection of oocytes was performed as described previously (20).

Data acquisition

Current and voltage signals were collected using conventional two-electrode voltage clamp with an OC-725C amplifier (Warner Instruments, Handen, CT). Signals were digitized and acquired using a digidata 1440 A/D convertor and pClamp 10.2 software (Axon Instruments, Foster City, CA). In proline mutant channels, recordings were made with cells exposed to a modified ND96 solution that contained 30 mM $[K^+]$ (in mM: 69 NaCl, 30KCl, 5 HEPES, 0.5 $CaCl_2$, 1 $MgCl_2$, titrated to pH 7.4) so as to increase the driving force for ion flow. In all other cases, unless otherwise stated, standard ND96 (i.e., with 96 mM NaCl, 3 mM KCl) solutions were used. Where applicable, 0.5 mM $CdCl_2$ was added to the ND96 solution and perfused at a flow rate of 1 ml/min. Recording microelectrodes were made from borosilicate glass with a resistance of 0.2–2.0 MΩ when filled with 3 M KCl. Current signals were acquired at a sampling rate of 10 kHz and with a 4 kHz low-pass Bessel filter. Recordings were performed at 20–22°C.

Voltage protocols and data analysis

Data were analyzed using Clampfit 10.3 (Axon Instruments), SigmaPlot11 (Systat Software, San Jose, CA), or IGOR Pro (Wavemetrics, Lake Oswego, OR) software. Steady-state conductance-voltage (G-V) relationships were determined from peak tail currents recorded during a voltage step to −110 mV applied following 2 s depolarizing pulses (holding potential, −80 mV). Many proline mutant channels passed inward current at −80 mV. In these cases, a holding potential of −30 mV was used, because this correlated reasonably well with the reversal potential in the modified, 30 mM external $[K^+]$, ND96 solution. In all cases, peak tail current amplitudes were normalized to the maximum tail current amplitude. The relationship between the steady-state current activation, fluorescence changes or charge movement, and membrane voltage were fitted (where possible) with a Boltzmann function: $y = 1/(1 + \exp(V_{1/2}–V)/k)$, where y is the relative conductance, fluorescence or Q_{off} normalized with respect to maximal conductance, fluorescence or Q_{off}, $V_{1/2}$ is the voltage of half-activation, V is the test voltage, and k is the slope factor. Rectification factor was calculated as previously described (1) using: $R = I/Gn(V\text{-}Erev)$, where R is the rectification factor, I is the membrane current, G is the slope conductance calculated from the fully activated current-voltage relationship, n is the activation variable (which was set at 1.0 because data were collected from fully activated channels, i.e., following a voltage step to +60 mV), V is the test voltage, and E_{rev} is the measured reversal potential. To determine the rate of channel activation, an envelope of tails activation protocol was used. Peak tail currents at −110 mV were measured following step to +60 mV of varying duration (10–500 ms). The holding potential was −80 mV. Activation time course was derived from single exponential fits of data plotting the peak tail current against depolarizing pulse duration: tau was derived from, $f(t) = A*\exp(t/\tau) + C$, where A is the amplitude of the fit, t is time, τ is the time constant of activation, and C is the residual current. The time course of fluorescence change upon depolarization was derived from single exponential fits using the same equation. All data are expressed as mean ± SE. In the figures, arrows indicate the zero current level and dotted lines are to guide the eye. Voltage protocols are depicted in figures and described in detail in the figure legends.

VCF

The G516C mutation in the S3-S4 linker was introduced as a site for fluorophore labeling with the impermeant thiol-reactive fluorescent probe, tetramethylrhodamine-5-maleimide (TMRM; Invitrogen). To prevent possible modification of the fluorescence emission from G516C, two native extracellular cysteines in the S1-S2 linker (C445 and C449) were replaced with valine (21). Oocytes were labeled with 5 μM TMRM in a depolarizing

solution (in mM: 99 KCl, 1 $MgCl_2$, 5 HEPES, and 2 $CaCl_2$, titrated to pH 7.4) for 30 min at 10°C in the dark. Two-electrode VCF experiments were performed as described previously (20). Fluorescence-voltage (F-V) relationships were determined from fluorescence signal amplitude at the end of the test pulse.

Gating current measurement using cut-open oocyte voltage clamp

Cut-open voltage-clamp experiments were performed using a CA-1B amplifier (Dagan, Minneapolis, MN) with the vaseline gap technique (22). Data were digitized at 50 kHz, low-pass-filtered at 10 kHz (using an ITC-16 interface, HEKA Elektronics), and recorded using Patchmaster software (HEKA Elektronics). Gating current recordings were performed 4–6 days after oocyte RNA injection. Microelectrodes pulled from borosilicate glass had resistances of 250–500 kΩ when filled with 3 M KCl. Extracellular solution in the top and guard chambers contained (in mM): 120 TEA-MES, 10 HEPES, 2 Ca-MES (titrated to pH 7.4). The hERG blocker terfenadine (100 μM) was added to the external solution to inhibit ionic current. Internal solution contained (in mM): 120 TEA-MES, 10 HEPES, 2 EGTA (titrated to pH 7.4). Recording bath temperature was maintained at 21°C with a Peltier device run by a TC-10 temperature controller (Dagan). To achieve the cut-open configuration, 0.1% saponin was added to the bottom bath for 30–60 s to permeabilize the oocyte membrane. Upon electrical access, saponin was washed out and replaced with intracellular solution. Oocytes expressing WT or G516C hERG were held at a holding potential of −100 mV. Oocytes expressing I663P/G516C were held at 0 mV, because gating charge movement was apparent in the negative voltage range. Capacitative transients were partially compensated with amplifier's analog circuitry. Linear leak subtraction was performed online by using a P/-8 protocol. Typical non-leak-subtracted WT hERG gating current records are shown in Fig. S1 in the Supporting Material, along with examples of recordings from uninjected oocytes. On-gating currents ($I_{g,on}$) were evoked by 100 ms steps from the holding potential to test potentials from −90 to +50 mV for WT and G516C channels, or from −10 to −160 mV for I663P/G516C. Off-gating ($I_{g,off}$) currents were recorded for 100 ms upon return to the holding potential. Charge-voltage (Q_{off}/V) relationships were determined by integrating $I_{g,off}$ and plotting the off-gating charge (Q_{off}) against test potential.

RESULTS

Fig. 1 characterizes the effects of introducing the PVP motif into the S6 helix of hERG channels, by the triple mutation I655P/F656V/G657P, on activation, deactivation, and inactivation gating properties. Fig. 1, *A–C*, compare the relative open probability of WT and PVP mutant channels over a range of voltages. Typical WT currents recorded in response to depolarizing voltage steps from a holding potential of −80 mV are shown in Fig. 1 *A*. Normalized peak tail current amplitudes in response to repolarization to −110 mV were used to plot the voltage-dependence of channel activation (Fig. 1 *C*). These WT data show that the relative open probability is low at −80 mV (relative $P_{o\text{-}80\ mV} = 0.02 \pm 0.01$) and maximal at +40 mV, and that the relationship between voltage and open probability is well described by a Boltzmann function ($V_{1/2}$ −27.4 ±1.4 mV; k 8.7 ± 0.1 mV; $n = 6$). Fig. 1 *B* shows typical hERG PVP currents recorded in response to voltage steps from −140 to +40 mV followed by repolarization to −110 mV (holding potential, −30 mV, see Materials and Methods). In contrast to WT channels, the normalized peak tail current amplitudes from hERG PVP channels (Fig. 1 *C*) show that the mutant channels are trapped in the open state over a wide range of voltages, passing inward current at hyperpolarized potentials (relative $P_{o\text{-}110\ mV} = 0.91 \pm 0.02$, $n = 4$) that did not appear to deactivate.

Fig. 1, *D–I*, suggest that the effects of the PVP substitution are limited to the open-closed equilibrium, because hERG PVP channels display strong inward rectification that is abolished by the S620T pore mutation, which inhibits inactivation. Fig. 1, *D* and *E*, show WT and PVP mutant channel tail currents in response to steps to a range of potentials following a 500 ms pulse to +60 mV to maximally activate the channels. In Fig. 1, *G* and *H*, the peak tail current amplitude is plotted as a function of test voltage. Strong rectification was observed in both WT and PVP mutant channels. To quantify and compare rectification in the two channel types, we calculated the rectification factor (Fig. 1 *I*; see Materials and Methods) from the fully activated tail current data in Fig. 1, *D* and *E*. The data were fitted with a Boltzmann function, which described similar voltage dependencies of rectification in the two channels: the $V_{1/2}$ of WT rectification was −61.7 ± 2.9 mV compared with −64.6 ± 1.0 mV in PVP channels (although the slope factor, k, was altered: k was 16.4 ± 0.3 and 8.8 ± 0.9 mV, respectively). In WT hERG channels, rectification can be abolished by the outer pore S620T mutation, which inhibits inactivation (23). Fig. 1, *F* and *H*, show that the S620T mutation also largely abolished rectification in hERG PVP channels. Taken together, the data shown in Fig. 1 indicate that inactivation is preserved in hERG PVP channels and that the predominant effect of the substitution is on the activation gate, biasing the open-closed equilibrium in favor of the open state.

We exploited the trapped-open phenotype observed following the PVP substitution within S6 to investigate the location of the pore gate. Our rationale was that the PVP mutation prevented the intracellular pore gate from closing by introducing a kink in the lower portion of S6 that reoriented the helices such that tight steric closure of the gate was prevented. Alternatively, the mutation could have disrupted the mechanical coupling of the gate with the voltage sensor, rendering it nonresponsive to changes of transmembrane potential. We hypothesized that by scanning down the S6 helix with single proline mutations a point would be reached at which proline introductions would no longer trap channels open, because the substituted site occupied a position below the gate. A similar approach was used previously to define the location of the gate in Kir3.4 inward rectifier channels, which also lack the PVP motif (24). Fig. 2 shows the results of the individual proline scan of S6 on hERG channel gating. Fig. 2, *A* and *B*, illustrates typical currents recorded from substitutions that trapped the hERG channel gate open (I663P) or did not markedly affect gating

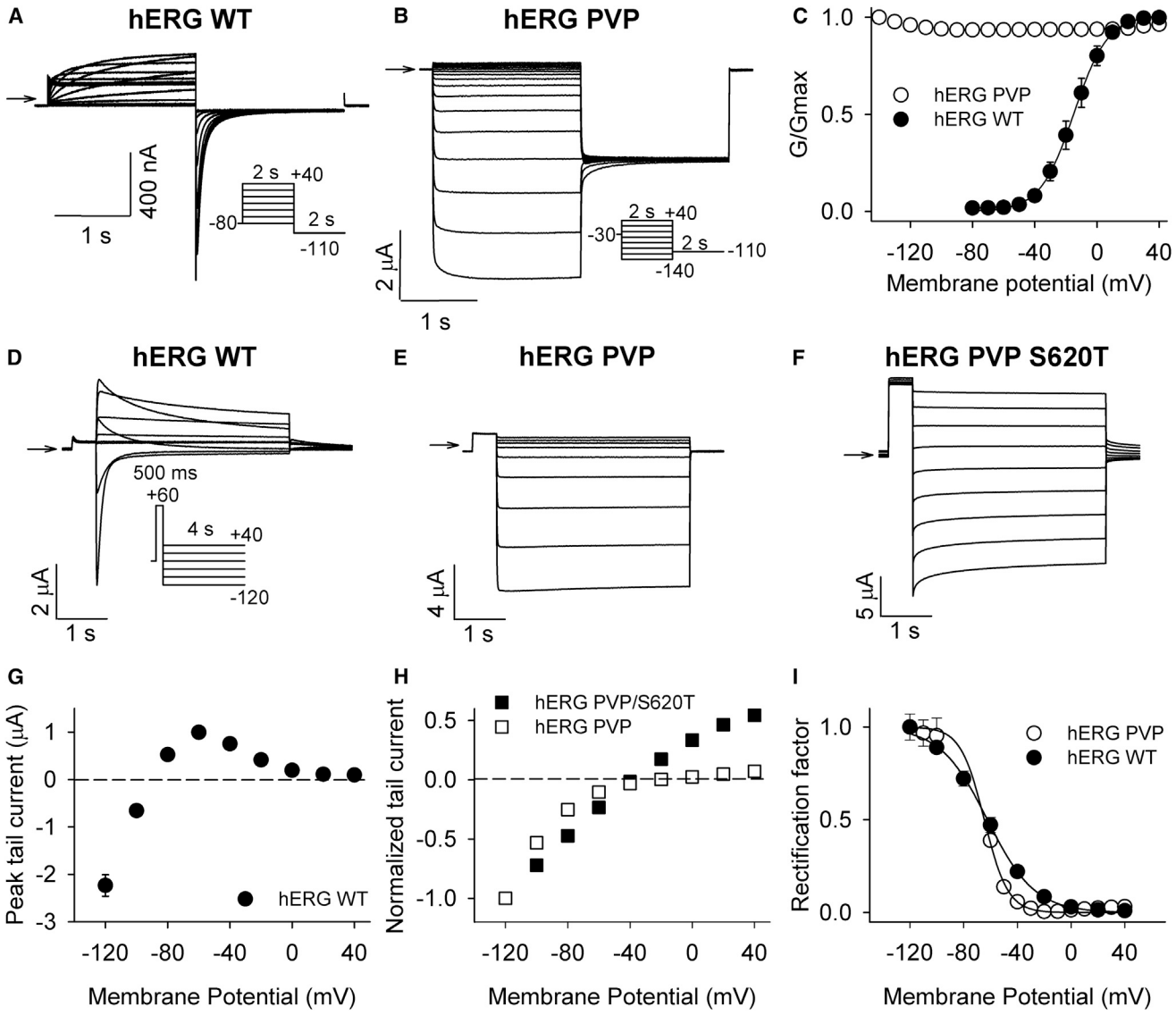

FIGURE 1 Introduction of the PVP motif perturbs the activation gate, but not inactivation. (*A* and *B*) Typical current traces from WT (*A*) and PVP mutant (*B*) channels evoked during 2 s depolarizing voltage steps from −80 mV (or from −140 mV in the case of PVP) to +40 mV (in 10 mV increments) followed by a 2 s hyperpolarizing step to −110 mV. Because PVP channels were trapped open, a holding potential of −30 mV was used as this approximated the reversal potential. WT currents were recorded in ND96 solution and from a holding potential of −80 mV. (*C*) Mean WT ($n = 6$) and PVP mutant ($n = 4$) G-V relations constructed from peak tail current amplitudes. G/G_{max} reflects the relative conductance at each voltage normalized to that +40 mV. WT, but not PVP mutant, data could be fitted with a Boltzmann function, which yielded values of −27.4 ± 1.4 and 8.7 ± 0.1 mV for $V_{1/2}$ and k, respectively. (*D–F*) Typical current traces from WT, PVP, and PVP/S620T channels evoked during 4 s repolarizing voltage steps from +40 to −120 mV applied following a 500 ms step to +60 mV to activate channels (holding potential was −80 mV for WT and −30 mV for PVP and PVP/S620T). (*G* and *H*) Fully activated WT (*G*), PVP (*H*) and PVP/S620T (*H*) instantaneous tail current voltage relations. Current amplitudes were normalized in (*H*) to compare rectification in the two constructs. (*I*) Rectification factor for WT and PVP channels calculated from the data in *G* and *H* (see Materials and Methods) as a measure of the voltage-dependence of inactivation in each channel. Data were fitted with a Boltzmann function. $V_{1/2}$ and k values were −61.7 ± 2.9 and 16.4 ± 0.3 mV for WT ($n = 8$), and −64.6 ± 1.0 and 8.8 ± 0.9 mV for PVP ($n = 3$), respectively.

(L666P). It is clear that I663P channels conduct robust currents during hyperpolarization as if the pore activation gate was trapped open and that the tail currents report maximal channel opening at all test potentials from −140 mV to +40 mV. In contrast, L666P channels were closed at −80 mV and only activated upon depolarization. As in WT channels, repolarization of L666P channels to −110 mV produced large transient tail currents indicative of channel closing during deactivation. Fig. 2 *C* demonstrates mean I663P and L666P G-V relations. The results from each site studied in the proline scan are summarized in Fig. 2 *D*. Here, the relative open probability is plotted for WT, the PVP mutant, and each individual proline substitution, from I655P to Y667P. We found a clear pattern to the

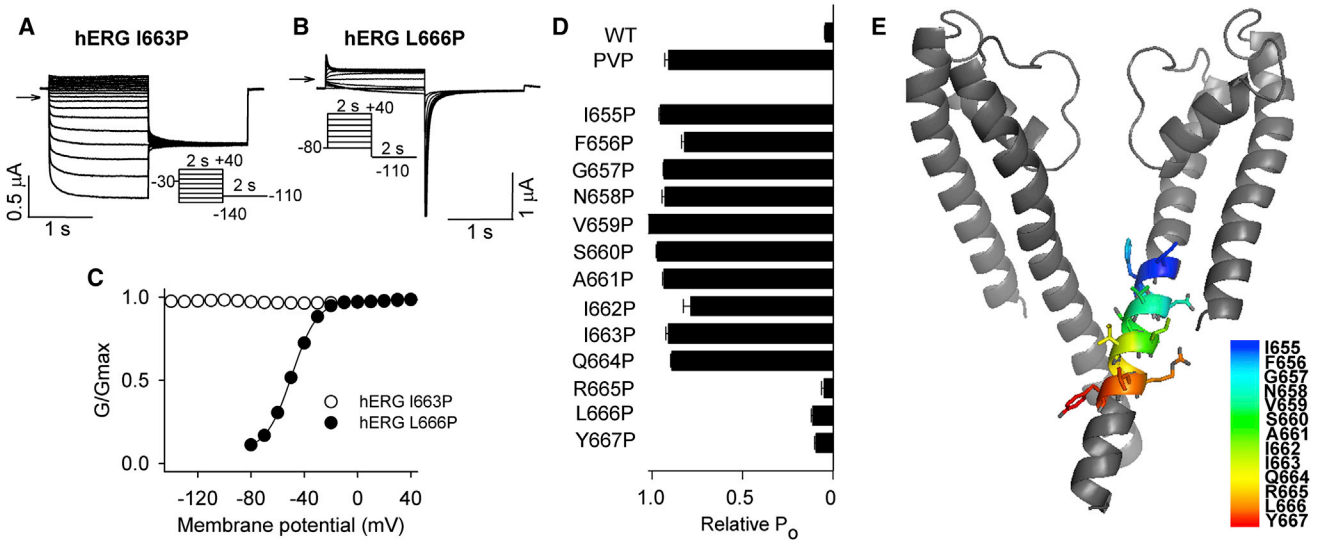

FIGURE 2 Mapping the location of the hERG channel pore gate using a proline scan. (*A* and *B*) Typical hERG I663P (*A*) and L666P (*B*) current traces evoked by 2 s voltage steps from –140 mV (or from −80 mV in the case of L666P) to +40 mV followed by a 2 s repolarizing step to −110 mV. (*C*) Mean L666P ($n = 6$) and I663P mutant ($n = 4$) G-V relations constructed from peak tail current amplitudes. G/G_{max} reflects the relative conductance at each voltage normalized to that +40 mV. L666P, but not I663P mutant, data could be fitted with a Boltzmann function, which yielded values of −51.2 ± 0.5 and 11.2 ± 0.3 mV for $V_{1/2}$ and k, respectively. (*D*) Plot of the relative open probability (P_o) for WT, the PVP mutant, and each of the individual proline substitutions from I655P to Y667P ($n = 5$). P_o values were calculated from G-V curves constructed as in Figs. 1 *C* and 2 *C*. For WT and WT-like gating mutants, the P_o at −80mV was used and for trapped-open mutants, the relative conductance at −110 mV was used. (*E*) Homology model of the hERG pore region (based on the MlotiK1 structure; coordinates from (18)) with inner S6 residues Ile^{655} to Tyr^{667} highlighted.

effects of proline introductions within S6, with proximal substitutions (Q664P and above) trapping channels open, as in the PVP mutant, and distal substitutions (R665P and below) preserving WT-like activation gate function (see Table S1). Fig. 2 *E* shows a homology model of the hERG channel pore with the region scanned by proline substitutions highlighted. That proline residues at and below Arg^{665} did not alter closing, whereas all residues above disrupted normal gate function, strongly suggests that the position of the intracellular gate lies at Gln^{664}.

Fig. 3 presents more detailed information of the gating behavior observed in each of the proline mutant channels. In Fig. 3 *A* typical traces recorded in response to a range of potentials following depolarization to +60 mV are shown. It is clear that R665P, L666P, and Y667P showed WT-like deactivation properties (see also Table S1), whereas proline substitutions at Gln^{664} and above exhibited very little closing even with a 4 s voltage step to −110 mV. Interestingly, the extent of closing in these cases was variable. For example, deactivation was negligible in G657P, S660P, and I663P channels, but more pronounced in I662P (although significant inward current remained after 4 s). In Fig. 3 *B*, the percentage deactivation observed at the end of 4 s repolarizing pulses to different potentials is plotted for each mutant. Although this isochronal measurement may not reflect steady-state conditions in all mutants, these data nevertheless provide for meaningful comparison of the extent of deactivation across channels. Fig. 3 *B* illustrates that R665P, L666P, and Y667P channels, like WT, deactivate in a voltage-dependent fashion and that at potentials negative to −80 mV deactivation is essentially complete after 4 s. In contrast, deactivation was negligible at all test potentials in G657P, S660P, and I663P channels, and the remaining mutant channels (with the exception of V659P; see below) showed some deactivation at strongly hyperpolarized potentials as if the dependence on voltage were shifted to a more hyperpolarized range. These data suggest that G657P, S660P, and I663P mutations trap the hERG channel gate open, whereas I655P, F656P, N658P, A661P, I662P, and Q664P strongly bias the open-closed equilibrium toward the open state. Fig. 3 *C* shows the position of the S6 helix residues tested in a helical wheel representation. Interestingly, G657, S660, and I663 lie along the same face of the S6 helix as the pore-lining Phe^{656}, and are within two turns of one another, suggesting that a proline-induced kink in this defined locale induces the most severe disruption of gate closure.

Data for deactivation of V659P channels are not represented in Fig. 3 *B*, because this mutant displayed an unusual and interesting, phenotype. These channels appeared trapped open (Fig. 2 *D*), but upon strong hyperpolarization (≤ -90 mV) we observed a slow increase in inward current as if channels were slowly activating at these voltages. Such behavior is reminiscent of the well-studied hyperpolarization-induced activation of hERG D540K channels (25–28) and this prompted us to further characterize the putative slow activation observed in V659P channels. Fig. 4 *A* shows typical currents recorded from hERG

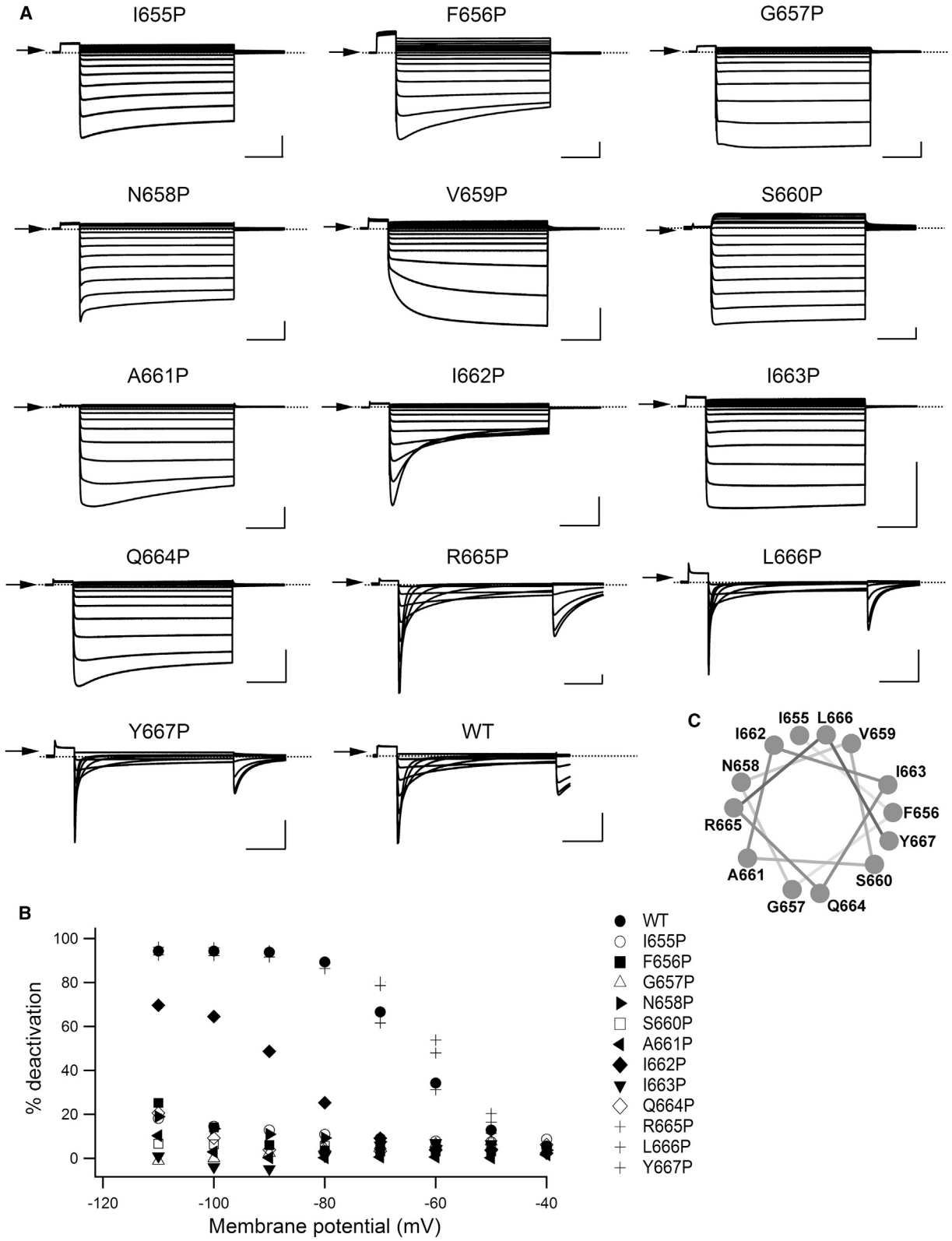

FIGURE 3 Proline substitutions in the inner S6 helix affect deactivation gating. (*A*) Typical current traces evoked from proline substitutions within the hERG S6 (I^{655} to Y^{667}) in response to 4 s voltage steps from −110 mV to +40 mV (or from −110 to −40 mV in the case of WT, R665P, L666P, Y667P) following a 500 ms depolarization to +60 mV. In each panel, scale bars represent 2 μA of current and 1 s time. (*B*) Plot of the percentage deactivation observed at the end of the 4 s repolarization for each mutant ($n = 5$–6). (*C*) Helical wheel representation showing the relative position of the inner S6 helix residues tested.

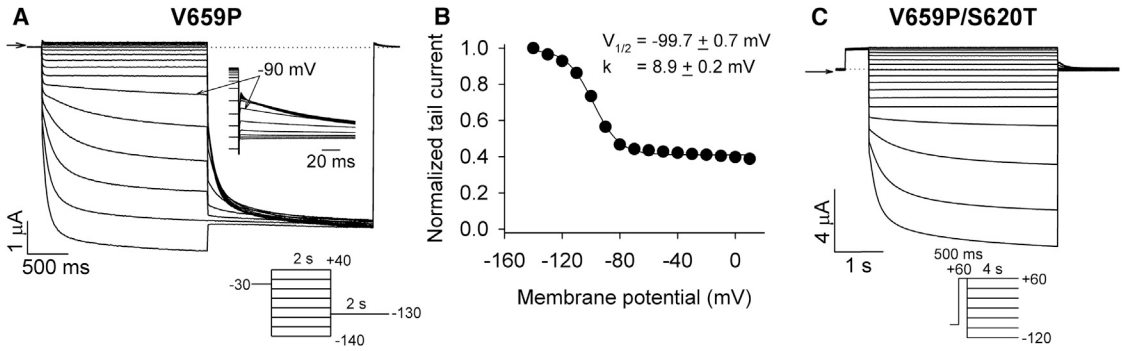

FIGURE 4 The V659P mutant is activated by hyperpolarization. (*A*) Typical hERG V569P current traces evoked from a holding potential of −30 mV in response to voltage steps applied from −140 mV to +40 mV, followed by a test pulse to −130 mV. The inset shows an expanded view of the tail currents recorded at −130 mV. (*B*), Plot of the dependence of the instantaneous tail current amplitude (recorded at −130 mV) on the preceding voltage step. Mean peak tail current amplitudes were normalized to the peak tail current recorded following a step to −140 mV ($n = 5$). Data were fitted with a Boltzmann function, which yielded values for $V_{1/2}$ and k of −99.7 ± 0.7 and 8.9 ± 0.2 mV, respectively. (*C*) Typical hERG V659P/S620T current traces evoked in response to 4 s hyperpolarizing steps from −120 to +60 mV following a 500 ms depolarization to +60 mV.

V659P channels in response to a protocol designed to measure the voltage dependence of the slowly activating current. In this protocol, voltage steps were applied from −140 mV to +40 mV and were followed by a step to −130 mV that allowed recovery from inactivation and quantification of the fraction of activated channels in the preceding pulse. Analysis of the current traces revealed that V659P, like other trapped-open proline mutant channels, pass inward non-deactivating current upon hyperpolarization between the holding potential (−30 mV) and −80 mV. However, unlike in any other proline mutant tested, further stronger hyperpolarization, i.e., −90 mV and more negative, induced a secondary slowly activating component of current in V659P channels that increased in amplitude with hyperpolarization such that it accounted for ~60% of the inward current at −140 mV. To quantify this, we plotted the peak tail current amplitude recorded at −130 mV in Fig. 4 *B* (*tail currents are shown on an expanded timescale in the inset* to Fig. 4 *A*). The slowly activating hyperpolarization-induced increase in V659P channel conductance was well described by a Boltzmann function with values for $V_{1/2}$ and k of −99.7 ± 0.7 and 8.9 ± 0.2 mV, respectively. Fig. 4 *C* shows that the hyperpolarization-activated conductance does not reflect altered recovery from inactivation, because the phenotype was preserved in hERG V659P/S620T channels in which inactivation is removed. These data suggest that the V659P mutation introduces a hyperpolarization-induced slow activation of channels, with a voltage dependence that is similar to that created by the hERG S4-S5 linker mutation, D540K (−117 mV (25,27,28)).

The mechanism by which voltage sensor coupling occurs with pore domains that lack the PVP motif is incompletely understood. We therefore investigated whether proline substitutions that trap open the activation gate (e.g., I663P) do so by altering the coupling between voltage sensor and pore. To assess this, we used two approaches to report on voltage sensor movement: VCF to provide a report on physical movements and gating current recordings using cut-open oocyte voltage clamp to provide a report on intramembrane charge movement (Fig. 5). Fig. 5 *A* shows typical fluorescence responses to changes in membrane voltage reported by TMRM attached at G516C in the S3-S4 linker (see Materials and Methods). This site was chosen as a site for TMRM-labeling, because it produced the most robust voltage-dependent fluorescence response of all cysteine introductions tested in this region (G516C-L520C; data not shown). The fluorescence change upon depolarization and repolarization is slow and is consistent with previous fluorescence reports from hERG L520C (21,29,30). Fig. 5 *B* compares the F-V relationship constructed from peak fluorescence measurements from G516C channels with the G-V relationship constructed from ionic tail current measurements. The F-V and G-V relationships had $V_{1/2}$ values of −27.0 ± 3.3 and −31.6 ± 1.9 mV, respectively, and k values of 15.8 ± 0.7 and 12.6 ± 0.7 mV. To correlate the fluorescence reports from G516C with the movement of gating charge, we recorded gating currents in both WT hERG and the G516C construct (Fig. 5 *C*). Both channels displayed qualitatively similar gating current profiles that are very similar to previously reported records from WT hERG expressed in *Xenopus* oocytes (31–34). We observed pronounced fast and slow on-gating current ($I_{g,on}$) components, the latter of which contributes most significantly to total charge movement (31–34), although, like others, we could not resolve the very fast component of charge movement reported from hERG channels expressed in human embryonic kidney cells (35). Integration of off-gating charge (Q_{off}) during a 100 ms repolarization step to −100 mV allowed comparison of the voltage-dependence of gating charge displacement with that of the fluorescence report from G516C channels (Fig. 5 *D*). In these experiments, the TMRM fluorophore attached at G516C in the S3-S4 linker of hERG reports reconfigurations occurring with a voltage-dependence that closely matches that of the bulk

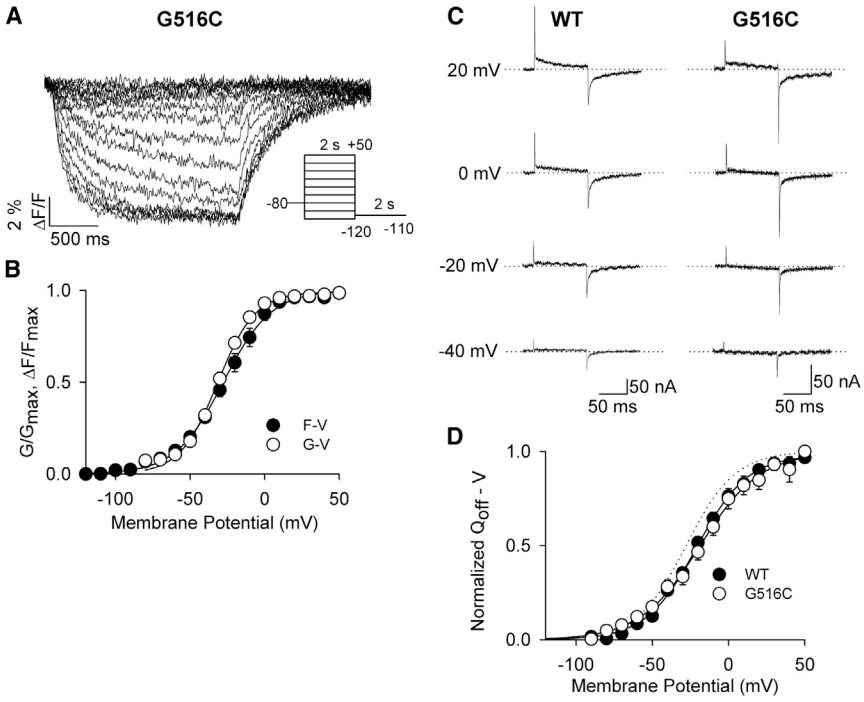

FIGURE 5 Reports of voltage sensor movement in hERG channels. (*A*) Typical fluorescence reports from TMRM-labeled hERG G516C channels evoked during 2 s voltage steps from −120 mV to +50 mV (*holding potential* −80 mV) followed by a 2 s repolarizing step to −110 mV. (*B*) Plot of mean G-V and F-V relations. G-V data derived from peak tail current amplitudes were normalized to the peak tail current following a step to +50 mV. F-V data derived from the fluorescence amplitude at the end of the 2 s depolarizing steps were normalized to the fluorescence amplitude at +50 mV. Data were fitted with a Boltzmann function. $V_{1/2}$ and k values were −31.6 ± 1.9 and 12.6 ± 0.7 mV for the G-V relation ($n = 5$), and −27.0 ± 3.3 and 15.8 ± 0.7 mV for the F-V relation ($n = 5$), respectively. (*C*) Typical WT and G516C gating currents evoked by 100 ms pulses to the indicated test voltages from a holding potential of −100 mV. (*D*) Mean Q_{off} -V relationships for the two channels constructed from normalized $I_{g,off}$ records. Data were fitted with a Boltzmann function. $V_{1/2}$ and k values were −20.9 ± 2.4 and 17.9 ± 1.5 mV for WT ($n = 7$), and −16.1 ± 4.4 and 21.7 ± 2.0 mV for G516C ($n = 7$), respectively. The dashed line represents the F-V relation of hERG G516C shown in panel *B*.

of gating charge movement, which approximates that of the G-V relationship. Recently, the slow movement of the bulk of gating charge was shown to precede, in kinetic terms, opening of the pore gate (32). Therefore, as a further test of whether the fluorescence report from G516C reflects voltage sensor movement, we measured the kinetics of the fluorescence change upon depolarization and compared this with the kinetics of pore opening recorded from a standard envelope of tails experiments (see Materials and Methods). The TMRM fluorescence report from hERG G516C channels activated with a tau of 55.9 ± 3.3 ms at +60 mV ($n = 5$), whereas pore gate activation occurred with a tau of 98.6 ± 4.1 ms at +60 mV ($n = 4$). These data support the idea that the fluorescence report from G516C tracks the slowly moving bulk of voltage-sensor gating charge.

We next examined voltage sensor movement in the I663P/G516C construct, which displays the trapped-open phenotype, to understand whether the introduction of a proline kink in S6 alters the conformational changes in S4 associated with channel gating. Fig. 6 shows fluorescence and gating current records from I663P/G516C channels. Because gating charge movement was apparent in the negative voltage range, test pulses were applied from a holding potential of 0 mV. Consequently, for purposes of consistency, we also used a holding potential of 0 mV for the VCF experiments. Fig. 6 *A* shows typical fluorescence reports from TMRM-labeled I663P/G516C channels in response to 2 s steps to voltages ranging from 0 mV to −180 mV (in −20 mV increments). The fluorescence changes from I663P/G516C channels are similar to those from G516C in that depolarization induces quenching of the fluorophore signal and hyperpolarization causes dequenching. The voltage-dependence of the fluorescence report upon hyperpolarization from 0 mV is shown in Fig. 6 *B*. A Boltzmann fit yielded values of −111.0 ± 1.02 and 10.8 ± 0.3 mV for the $V_{1/2}$ and k, respectively. Gating current measurements during 100 ms hyperpolarizing steps from a holding potential of 0 mV (Fig. 6 *C*) confirm that the voltage-sensing domain in I663P/G516C channels is functional. $I_{g,on}$ and $I_{g,off}$ records were qualitatively similar to those of WT and G516C channels, but the voltage-dependence was shifted in the negative direction. The mean Q_{off} observed in seven oocytes is plotted against the hyperpolarizing step potential in Fig. 6 *D*. We were unable to reach saturating potentials for gating charge movement in this construct due to instability of the oocyte membrane and the presence of endogenous chloride currents at potentials more negative than −160mV and therefore the data could not be fitted with a Boltzmann function. Despite this, the observed voltage-dependence of gating charge appears to correlate reasonably well with the voltage-dependence of fluorescence changes (Fig. 6 *B*).

As further confirmation that the fluorescence report from I663P/G516C channels reflected conformational changes of the voltage sensor, we used Cd^{2+} as a tool, because it is known to shift the voltage-dependence of gating charge movement to more positive potentials, as well as to slow the development of the on-gating charge and accelerate

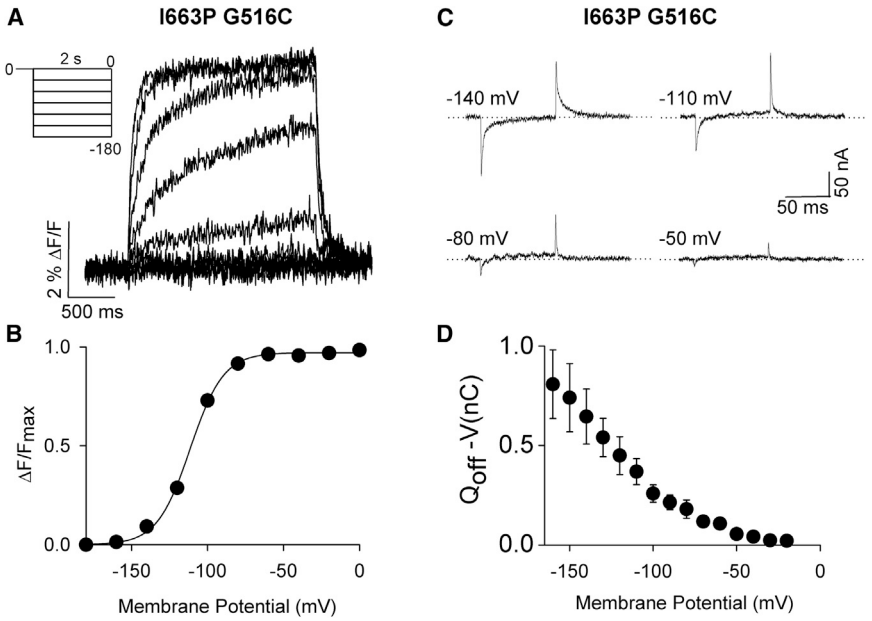

FIGURE 6 Detection of voltage sensor movement in trapped-open hERG channels. (*A*) Typical fluorescence reports from TMRM-labeled hERG I663P/G516C channels evoked during 2 s voltage steps from a holding potential of 0 mV to −180 mV in 20 mV increments. (*B*) Mean F-V ($n = 5$) relation from I663P/G516C fluorescence. Data were fitted with a Boltzmann function, which yielded $V_{1/2}$ and k values of −111.0 ± 1.0 and 10.8 ± 0.3 mV, respectively. (*C*) Typical hERG I663P/G516C gating currents evoked by 100 ms pulses to the indicated test voltages from a holding potential of 0 mV. (*D*) Mean Q_{off}-V relationship ($n = 7$) constructed from integration of $I_{g,off}$ over time.

that of the off-gating charge (31). Fig. 7 *A* displays typical fluorescence reports from I663P/G516C channels in the absence and presence of 0.5 mM Cd^{2+} (close to the reported IC_{50} (31)). In these experiments, a 2 s voltage step from the holding potential of −30 mV to −120 mV (P1) reported voltage sensor movement during deactivation, and this was followed by voltage steps from −180 to 0 mV (P2) to study the voltage-dependence of activation. It is clear that the fluorescence report upon hyperpolarization to −120 mV (P1) was accelerated in the presence of Cd^{2+}, consistent with the acceleration of the off-gating charge reported previously (31). Fig. 7 *B* shows plots of F-V relations measured from peak fluorescence amplitudes during P2, and G-V relations measured with the protocol described in Fig. 2 *A*, in the absence and presence of Cd^{2+}. Conductance-voltage relationships confirm that Cd^{2+} does not affect the trapped-open pore at any voltage in the range studied (−140mV to +40mV). Boltzmann fits of fluorescence data yielded $V_{1/2}$ and k values of −86.1 ± 2.6 and 14.4 ± 1.0 mV under control conditions and −53.7 ± 0.8 and 13.9 ± 0.8 mV with 0.5 mM Cd^{2+}. The ~30 mV right-shift of the fluorescence report in the presence of 0.5 mM Cd^{2+} is entirely consistent with the reported effects on the voltage-dependence of gating charge movement (31). Taken together, the data in Figs. 6 and 7 indicate that the fluorescence report from G516C tracks the voltage sensor movement in the trapped-open I663P channels. The data from both fluorescence and intramembrane charge movement measurements suggest that introduction of a proline-induced kink in the S6 helix disrupts the electromechanical coupling of S4 with the pore gate such that the gate is effectively isolated and trapped in the open conformation.

Characterization of channels in which voltage sensor movement is uncoupled from pore opening, e.g., *Shaker*

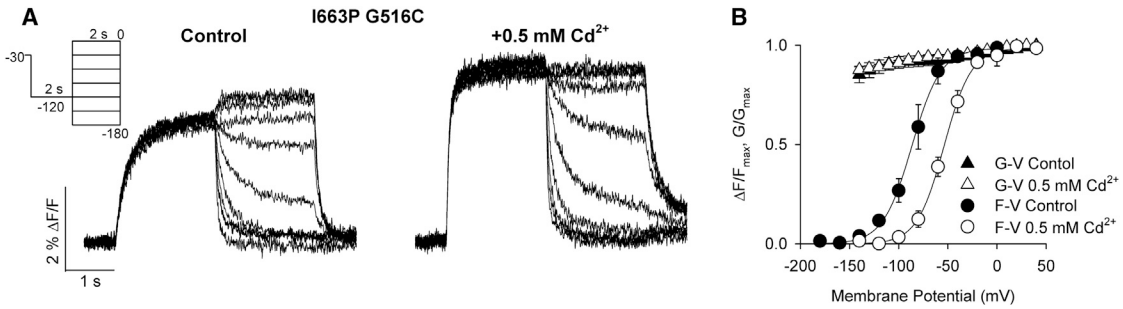

FIGURE 7 Effect of Cd^{2+} on the fluorescence report of voltage sensor movement. (*A*) Typical fluorescence reports from TMRM-labeled hERG I663P/G516C channels in the absence and presence of 0.5 mM Cd^{2+}. Fluorescence reports were evoked during 2 s steps to voltages from 0 to −180 mV in 20 mV increments, following a 2 s prepulse to −120 mV from a holding potential of −30 mV. (*B*) Comparison of mean G-V and F-V relations in the absence and presence of 0.5 mM Cd^{2+}. G-V relations were constructed from peak tail current amplitudes as in Fig. 2 *A* both in control ($n = 4$) and in the presence of 0.5 mM Cd^{2+} ($n = 4$), respectively. F-V data were fitted with a Boltzmann function, which yielded $V_{1/2}$ and k values of −86.1 ± 2.6 and 14.4 ± 1.0 mV in control ($n = 5$), and −53.7 ± 0.8 and 13.9 ± 0.8 mV in the presence of 0.5 mM Cd^{2+} ($n = 5$), respectively.

ILT, has proven valuable in understanding the mechanisms of voltage-dependency in ion channels (36–39). Similar tools for dissociating gating steps in the activation pathway of hERG channels have, however, been less forthcoming. Fig. 8 *A* plots the voltage-dependence of the fluorescence report of voltage sensor movement from G516C with and without the I663P mutation on the same axes (data from Figs. 5 *B* and 7 *B*). The I663P mutation resulted in a left-shifted dependence of voltage sensor activation on membrane potential. Fig. 8 *B* compares the time course of voltage sensor activation and deactivation as reported by fluorescence in I663P/G516C channels. Voltage sensor activation tau values are also plotted for G516C channels for purposes of comparison. In both cases, voltage sensor activation tau values report relatively slow activation. These data indicate that after accounting for the shift in the voltage-dependence, the rate of voltage sensor activation is similar in channels in which coupling with the pore is intact (G516C) or perturbed (I663P/G516C). This result suggests that the slow charge movement observed in hERG channels expressed in *Xenopus* oocytes (Figs. 5 *C* and 6 *C*, see also (31–34)) is an intrinsic property of the voltage-sensing unit and does not appear to be imparted by its coupling to the pore.

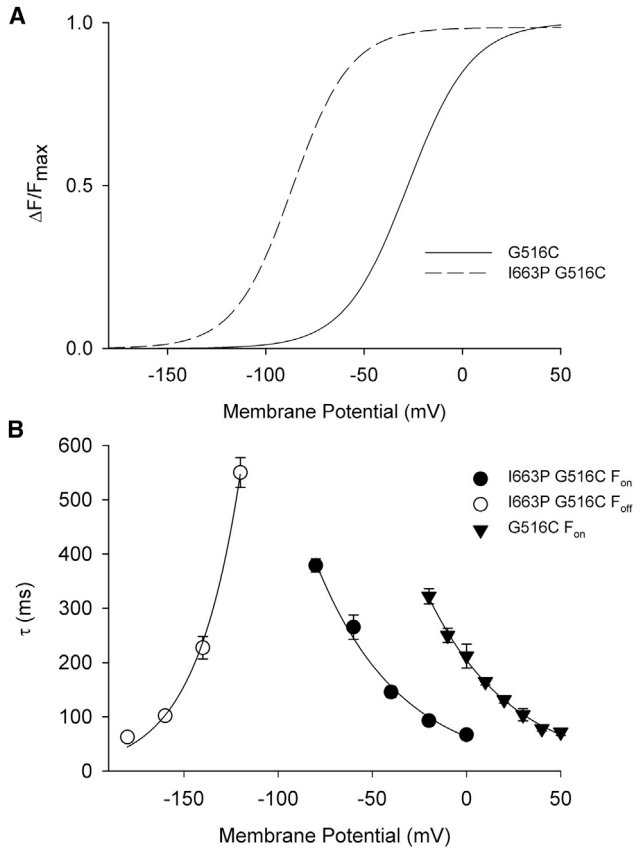

FIGURE 8 Characteristics of voltage sensor movement with disrupted coupling to the pore. (*A*) Comparison of the voltage-dependence of the fluorescence report of voltage sensor movement in G516C channels with and without the I663P mutation, which disrupts the coupling of the voltage sensor with the pore gate. Data taken from Figs. 5 *B* and 7 *B* are compared on the same axes. (*B*) Mean tau values from single exponential fits of fluorescence signals from G516C during depolarizing voltage steps in the absence and presence of the I663P mutation using: $f(t) = A^{*}\exp(-t/\tau) + C$, where A is the amplitude of the fit, t is time, τ is the time constant of deactivation, and C is the residual current. Tau values from fits of fluorescence changes during deactivation in I663P/G516C channels are also shown.

DISCUSSION

Location of the hERG activation gate

In this study, we have used a proline scan approach to define the location of the intracellular activation gate in hERG channels. Prolines substituted at or above Gln^{664} trapped channels in the open state, whereas substitutions below (at Arg^{665}, Leu^{666}, Tyr^{667}) showed WT-like activation and deactivation properties (Figs. 2 and 3, Table S1), suggesting that the gate is formed at Gln^{664}. A similar proline scan approach was previously used to identify the location of the intracellular activation gate in Kir3.4 inward rectifier channels (24), which, like hERG, lack the PVP motif. In Kir3.4 channels, introduction of proline residues on the outer face of S6 resulted in constitutively activated channels, whereas proline substitutions on the inner face trapped the pore closed (24). Molecular modeling suggests that introduction of proline creates a kink in the helix that may have bent the lower portion away from the permeation pathway, trapping the activation gate in the open state (24). The structural consequences of proline residues within an α-helix are well described; avoidance of steric clashes with i - 4 (where the proline is at position i) and the loss of hydrogen bonds with i - 3 and i - 4 increase helix flexibility N-terminal to the proline favoring a kink of ~20° away from the helix axis (40–43). Given this, it is reasonable to conclude that the proline substitutions in hERG (and Kir3.4) induce a kink that reorients the S6 helix N-terminal to the introduced proline residue. Surprisingly, our results in hERG demonstrate that all proline substitutions from Ile^{655} to Gln^{664} disrupted pore gate closing suggesting that these sites lie above the steric constriction site of the gate. In contrast, our data indicate that Arg^{665}, Leu^{666}, and Tyr^{667} are below the gate, because they do not impede gate closure.

In the majority of cases a proline-induced α-helical kink occurs within i - 4 and i (40–43). Our functional data suggest that a proline at Gln^{664} marks the boundary of gate disruption and we have interpreted this to imply that Gln^{664} forms the gate, just as the PVP-induced kink in *Shaker*-like channels is often referred to as the activation gate. This would place the gate more than one helical turn below that described in Kir3.4 (24) and *Shaker* (11,12) channels and is consistent with previous predictions of hERG activation gate architecture (18). These predictions were made based on cysteine substitution data, which showed that cysteines at specific positions within S6 induced a standing conductance

at hyperpolarized potentials, as if channel closure were impeded (18). When the sites affected were mapped onto a structural model constructed using the MlotiK1 cyclic nucleotide gated channel, the data suggested that Gln^{664} may create the steric barrier that occludes ion flow leading the authors to predict that Gln^{664}, Tyr^{667}, and Ser^{668} may form a gate at a position that is one helical turn lower in hERG than in *Shaker* channels. Our functional data using an alternative approach support and confirm that Gln^{664} likely forms the intracellular activation gate in hERG channels and that the gate position is lower in S6 than in other K^+ channels, such as *Shaker* and Kir3.4.

Proline substitutions within S6 that trapped the activation gate open did so with minimal effect on inactivation gating. However, we did observe a steeper voltage-dependence of inactivation in hERG PVP (and hERG I663P; data not shown) mutant channels compared to WT (Fig. 1 *I*). These data suggest that the voltage sensitivity of inactivation may be enhanced in trapped-open channels. This requires further study, however, because inactivation in hERG channels is not strongly coupled to activation and the derivation of its unusual dependence upon voltage is unclear. For example, some evidence suggests that a microdomain of S4 imparts inactivation voltage dependence (33), whereas other data suggest a role for the S5-P turret region (44–46). More recently, more global complex rearrangements throughout the channel that are initiated by K^+ exit from the pore have been proposed to regulate inactivation in hERG channels (47). Although strong conclusion cannot be drawn from the data in this regard, they demonstrate that inactivation is conserved in the trapped-open channels.

Disruption of coupling between the voltage sensor and the pore

It is interesting to note that all proline substitutions above the gate trapped channels open, rather than producing a α-helical pattern where prolines on one face of the helix stabilized the open gate and those on the opposite side stabilized the closed gate, as was observed in Kir3.4 (24). We interpret this to mean that any proline-induced perturbation of the S6 helix, no matter the orientation, disrupts gate closure. Although, the peculiar kinetics of mutants such as F656P, V659P, and I662P suggests that individual positions of proline substitutions have specific effects on the ability of the modified pore gate to approach steric closure, i.e., a nonconducting conformation. One possibility is that proline mutant channels are trapped open because the mutations immobilize the voltage sensor in the activated up configuration. In this case the voltage sensors would not respond to changes in membrane potential and channels would not close upon hyperpolarization. However, our fluorescence and gating current reports (Figs. 5–7) show intact voltage sensor movement in I663P trapped-open channels. The close correlation of our intramembrane charge measurements and fluorescence signals in the same construct (Figs. 6 and 7) suggest that both approaches report upon voltage sensor movement. The demonstration that the fluorescence signals are also manipulated by Cd^{2+} (Fig. 7), well known to specifically coordinate with and modify voltage sensor behavior (31), provides further support for this conclusion. In addition, our fluorescence data from G516C show that the fluorescence report of voltage sensor movement occurs with a similar voltage-dependence to that of pore opening, but precedes, kinetically, opening of the pore gate. These data are consistent with a recent comparison of hERG gating currents recorded with cut-open voltage clamp (32) and whole cell patch clamp in mammalian cells (35), which showed that a prominent slow phase of voltage sensor movement carries the bulk of charge that moves ahead of, but with a voltage-dependence that is similar to that of channel opening. Finally, our data showing voltage-dependent fluorescence signals that correlate with gating currents in I663P channels, which do not show any signs of pore constriction at the activation gate strengthen the notion that fluorophore probes attached to S3-S4 linker residues report local rearrangements of the voltage sensor.

Taken together, we interpret our data to indicate that the S6 proline mutations disrupt the coupling of the voltage sensor movement to the intracellular pore activation gate. Such disruption may occur by structurally perturbing the interaction between the S4-S5 linker and lower S6 so that S4 motion is no longer electromechanically coupled to the pore, or by altering the structure of S6 so that S4-S5 linker work applied during repolarization is not sufficient, or is not applied in the appropriate direction, to actuate closure of the permeation pathway gate.

Voltage sensor movement in the absence of normal coupling to the pore gate

We observed fluorescence changes and gating currents from I663P/G516C channels, in which the activation gate is trapped open, that were similar to those from G516C channels, in which normal gate function is preserved, although with altered voltage-dependence (Fig. 8). This supports the previous suggestion (30) that fluorescence signals from the hERG S3-S4 linker report on voltage sensor conformational changes that are distinct from pore opening. Observation of the fluorescence signal characteristics in I663P channels allows scrutiny of voltage sensor movement in the absence of normal coupling to the pore. The data in Fig. 8 *B* indicate that slow voltage sensor activation is an intrinsic property of the voltage-sensing unit of hERG.

Hyperpolarization-induced activation in V659P channels

The V659P mutant phenotype was of particular interest and warranted further investigation (Fig. 4). This mutant

channel passed robust inward current at −80 mV, just as in other trapped open proline mutant channels; however, upon stronger hyperpolarizing steps of ≤−90 mV an additional slowly activating voltage-dependent conductance was evident. These data are strikingly similar to hyperpolarization-activated cyclic nucleotide gated channel gating and are also reminiscent of the hERG D540K S4-S5 linker mutant phenotype, which reopens into a hyperpolarized activated state (26–28), as well as the hyperpolarization-activated conductance induced in NaChBac channels containing S6 proline substitutions (48). These data suggest that the substituted proline at V659 creates an additional open state that is accessed upon strong hyperpolarization ($V_{1/2} = -99.7$ mV) and that is distinct from the open state occupied at potentials more positive than −80 mV. A similar two open-state model has been proposed for hERG D540K channels (27).

CONCLUSION

From these studies, we conclude that the location of the intracellular gate in hERG channels is at Gln^{664}, at least one helical turn below that in *Shaker* channels. Proline introductions at or above this position disrupt the coupling of the pore gate from the voltage sensor movement, trapping channels in the open state. VCF and gating currents from these trapped-open channels suggest that voltage sensor movement is intrinsically slow in hERG channels.

SUPPORTING MATERIAL

One figure and one table are available at http://www.biophysj.org/biophysj/supplemental/S0006-3495(14)00137-4.

The authors acknowledge Ji Qi and Charlene Allard for technical support.

This study was supported by a Grant-in-aid from the Heart and Stroke Foundation of British Columbia and Yukon (T.W.C.) and a Canada Foundation for Innovation Leader's Opportunity Fund (T.W.C). T.W.C was supported by a Heart and Stroke New Investigator Award and a Michael Smith Foundation for Health Research Career Scholar Award. Y.M.C was supported by a Postdoctoral Scholarship from the Heart and Stroke Foundation of Canada.

REFERENCES

1. Sanguinetti, M. C., C. Jiang, …, M. T. Keating. 1995. A mechanistic link between an inherited and an acquired cardiac arrhythmia: HERG encodes the IKr potassium channel. *Cell.* 81:299–307.
2. Trudeau, M. C., J. W. Warmke, …, G. A. Robertson. 1995. HERG, a human inward rectifier in the voltage-gated potassium channel family. *Science.* 269:92–95.
3. Curran, M. E., I. Splawski, …, M. T. Keating. 1995. A molecular basis for cardiac arrhythmia: HERG mutations cause long QT syndrome. *Cell.* 80:795–803.
4. Sanguinetti, M. C., M. E. Curran, …, M. T. Keating. 1996. Spectrum of HERG K^+-channel dysfunction in an inherited cardiac arrhythmia. *Proc. Natl. Acad. Sci. USA.* 93:2208–2212.
5. Durdagi, S., J. Guo, …, H. J. Duff. 2012. Structure-guided topographic mapping and mutagenesis to elucidate binding sites for the human ether-a-go-go-related gene 1 potassium channel (KCNH2) activator NS1643. *J. Pharmacol. Exp. Ther.* 342:441–452.
6. Armstrong, C. M. 1966. Time course of TEA^+-induced anomalous rectification in squid giant axons. *J. Gen. Physiol.* 50:491–503.
7. Armstrong, C. M. 1971. Interaction of tetraethylammonium ion derivatives with the potassium channels of giant axons. *J. Gen. Physiol.* 58:413–437.
8. Armstrong, C. M., and B. Hille. 1972. The inner quaternary ammonium ion receptor in potassium channels of the node of Ranvier. *J. Gen. Physiol.* 59:388–400.
9. Holmgren, M., P. L. Smith, and G. Yellen. 1997. Trapping of organic blockers by closing of voltage-dependent K^+ channels: evidence for a trap door mechanism of activation gating. *J. Gen. Physiol.* 109:527–535.
10. del Camino, D., and G. Yellen. 2001. Tight steric closure at the intracellular activation gate of a voltage-gated K^+ channel. *Neuron.* 32:649–656.
11. Liu, Y., M. Holmgren, …, G. Yellen. 1997. Gated access to the pore of a voltage-dependent K^+ channel. *Neuron.* 19:175–184.
12. Hackos, D. H., T. H. Chang, and K. J. Swartz. 2002. Scanning the intracellular S6 activation gate in the shaker K^+ channel. *J. Gen. Physiol.* 119:521–532.
13. Kitaguchi, T., M. Sukhareva, and K. J. Swartz. 2004. Stabilizing the closed S6 gate in the *Shaker* Kv channel through modification of a hydrophobic seal. *J. Gen. Physiol.* 124:319–332.
14. Doyle, D. A., J. Morais Cabral, …, R. MacKinnon. 1998. The structure of the potassium channel: molecular basis of K^+ conduction and selectivity. *Science.* 280:69–77.
15. Jiang, Y., A. Lee, …, R. MacKinnon. 2002. The open pore conformation of potassium channels. *Nature.* 417:523–526.
16. Long, S. B., E. B. Campbell, and R. Mackinnon. 2005. Voltage sensor of Kv1.2: structural basis of electromechanical coupling. *Science.* 309:903–908.
17. Long, S. B., E. B. Campbell, and R. Mackinnon. 2005. Crystal structure of a mammalian voltage-dependent *Shaker* family K^+ channel. *Science.* 309:897–903.
18. Wynia-Smith, S. L., A. L. Gillian-Daniel, …, G. A. Robertson. 2008. hERG gating microdomains defined by S6 mutagenesis and molecular modeling. *J. Gen. Physiol.* 132:507–520.
19. Fernandez, D., A. Ghanta, …, M. C. Sanguinetti. 2004. Physicochemical features of the HERG channel drug binding site. *J. Biol. Chem.* 279:10120–10127.
20. Van Slyke, A. C., S. Rezazadeh, …, T. W. Claydon. 2010. Mutations within the S4-S5 linker alter voltage sensor constraints in hERG K^+ channels. *Biophys. J.* 99:2841–2852.
21. Es-Salah-Lamoureux, Z., R. Fougere, …, D. Fedida. 2010. Fluorescence-tracking of activation gating in human ERG channels reveals rapid S4 movement and slow pore opening. *PLoS. One.* 5:e10876.
22. Stefani, E., and F. Bezanilla. 1998. Cut-open oocyte voltage-clamp technique. *Methods Enzymol.* 293:300–318.
23. Ficker, E., W. Jarolimek, and A. M. Brown. 2001. Molecular determinants of inactivation and dofetilide block in ether a-go-go (EAG) channels and EAG-related K^+ channels. *Mol. Pharmacol.* 60:1343–1348.
24. Jin, T., L. Peng, …, D. E. Logothetis. 2002. The $\beta\gamma$ subunits of G proteins gate a K^+ channel by pivoted bending of a transmembrane segment. *Mol. Cell.* 10:469–481.
25. Ferrer, T., J. Rupp, …, M. Tristani-Firouzi. 2006. The S4-S5 linker directly couples voltage sensor movement to the activation gate in the human ether-a'-go-go-related gene (hERG) K^+ channel. *J. Biol. Chem.* 281:12858–12864.
26. Mitcheson, J. S., J. Chen, and M. C. Sanguinetti. 2000. Trapping of a methanesulfonanilide by closure of the HERG potassium channel activation gate. *J. Gen. Physiol.* 115:229–240.

27. Sanguinetti, M. C., and Q. P. Xu. 1999. Mutations of the S4-S5 linker alter activation properties of HERG potassium channels expressed in *Xenopus* oocytes. *J. Physiol.* 514:667–675.

28. Tristani-Firouzi, M., J. Chen, and M. C. Sanguinetti. 2002. Interactions between S4-S5 linker and S6 transmembrane domain modulate gating of HERG K^+ channels. *J. Biol. Chem.* 277:18994–19000.

29. Smith, P. L., and G. Yellen. 2002. Fast and slow voltage sensor movements in HERG potassium channels. *J. Gen. Physiol.* 119:275–293.

30. Tan, P. S., M. D. Perry, …, A. P. Hill. 2012. Voltage-sensing domain mode shift is coupled to the activation gate by the N-terminal tail of hERG channels. *J. Gen. Physiol.* 140:293–306.

31. Abbruzzese, J., F. B. Sachse, …, M. C. Sanguinetti. 2010. Modification of hERG1 channel gating by Cd^{2+}. *J. Gen. Physiol.* 136:203–224.

32. Goodchild, S. J., and D. Fedida. 2013. Gating charge movement precedes ionic current activation in hERG channels. *Channels (Austin).* 8:PM:24126078.

33. Piper, D. R., W. A. Hinz, …, M. Tristani-Firouzi. 2005. Regional specificity of human ether-a'-go-go-related gene channel activation and inactivation gating. *J. Biol. Chem.* 280:7206–7217.

34. Piper, D. R., A. Varghese, …, M. Tristani-Firouzi. 2003. Gating currents associated with intramembrane charge displacement in HERG potassium channels. *Proc. Natl. Acad. Sci. USA.* 100:10534–10539.

35. Wang, Z., Y. Dou, …, D. Fedida. 2013. Components of gating charge movement and S4 voltage-sensor exposure during activation of hERG channels. *J. Gen. Physiol.* 141:431–443.

36. Ledwell, J. L., and R. W. Aldrich. 1999. Mutations in the S4 region isolate the final voltage-dependent cooperative step in potassium channel activation. *J. Gen. Physiol.* 113:389–414.

37. Pathak, M., L. Kurtz, …, E. Isacoff. 2005. The cooperative voltage sensor motion that gates a potassium channel. *J. Gen. Physiol.* 125:57–69.

38. Smith-Maxwell, C. J., J. L. Ledwell, and R. W. Aldrich. 1998. Role of the S4 in cooperativity of voltage-dependent potassium channel activation. *J. Gen. Physiol.* 111:399–420.

39. Smith-Maxwell, C. J., J. L. Ledwell, and R. W. Aldrich. 1998. Uncharged S4 residues and cooperativity in voltage-dependent potassium channel activation. *J. Gen. Physiol.* 111:421–439.

40. Barlow, D. J., and J. M. Thornton. 1988. Helix geometry in proteins. *J. Mol. Biol.* 201:601–619.

41. Cordes, F. S., J. N. Bright, and M. S. Sansom. 2002. Proline-induced distortions of transmembrane helices. *J. Mol. Biol.* 323:951–960.

42. MacArthur, M. W., and J. M. Thornton. 1991. Influence of proline residues on protein conformation. *J. Mol. Biol.* 218:397–412.

43. von Heijne, G. 1991. Proline kinks in transmembrane alpha-helices. *J. Mol. Biol.* 218:499–503.

44. Clarke, C. E., A. P. Hill, …, J. I. Vandenberg. 2006. Effect of S5P alpha-helix charge mutants on inactivation of hERG K^+ channels. *J. Physiol.* 573:291–304.

45. Liu, J., M. Zhang, …, G. N. Tseng. 2002. Structural and functional role of the extracellular s5-p linker in the HERG potassium channel. *J. Gen. Physiol.* 120:723–737.

46. Torres, A. M., P. S. Bansal, …, J. I. Vandenberg. 2003. Structure of the HERG K+ channel S5P extracellular linker: role of an amphipathic alpha-helix in C-type inactivation. *J. Biol. Chem.* 278:42136–42148.

47. Wang, D. T., A. P. Hill, …, J. I. Vandenberg. 2011. Mapping the sequence of conformational changes underlying selectivity filter gating in the K(v)11.1 potassium channel. *Nat. Struct. Mol. Biol.* 18:35–41.

48. Zhao, Y., T. Scheuer, and W. A. Catterall. 2004. Reversed voltage-dependent gating of a bacterial sodium channel with proline substitutions in the S6 transmembrane segment. *Proc. Natl. Acad. Sci. USA.* 101:17873–17878.